Geophysical Research Letters

RESEARCH LETTER
10.1029/2024GL111897

Common and Distinct Drivers of Convective Mass Flux and Walker Circulation Changes

Sarah M. Kang[1], **Masahiro Watanabe**[2], **and Veronika Gayler**[1]

[1]Max Planck Institute for Meteorology, Hamburg, Germany, [2]Atmosphere and Ocean Research Institute, University of Tokyo, Kashiwa, Japan

Key Points:

- Convective mass flux weakens in proportion to the global warming amplitude, largely unaffected by SST pattern changes
- Walker circulation weakening due to global warming can be overcompensated by a sufficiently large increase in zonal SST gradient
- The weakening of convective mass flux alone is insufficient for explaining the Walker circulation response to global warming

Supporting Information:

Supporting Information may be found in the online version of this article.

Correspondence to:

S. M. Kang,
sarah.kang@mpimet.mpg.de

Citation:

Kang, S. M., Watanabe, M., & Gayler, V. (2025). Common and distinct drivers of convective mass flux and Walker circulation changes. *Geophysical Research Letters*, *52*, e2024GL111897. https://doi.org/10.1029/2024GL111897

Received 16 AUG 2024
Accepted 2 NOV 2024

Author Contributions:

Conceptualization: Sarah M. Kang, Masahiro Watanabe
Data curation: Veronika Gayler
Formal analysis: Sarah M. Kang
Investigation: Veronika Gayler
Methodology: Sarah M. Kang, Veronika Gayler
Visualization: Sarah M. Kang
Writing – original draft: Sarah M. Kang
Writing – review & editing: Sarah M. Kang, Masahiro Watanabe, Veronika Gayler

Abstract The weakening of convective mass flux and the Walker circulation is one of the most robust responses to global warming. However, recent decades have seen the Pacific Walker circulation strengthen despite a weakening convective mass flux. Here, we conduct a series of prescribed sea surface temperature (SST) experiments to separate the effects of global warming from changes in SST patterns. The tropical-mean convective mass flux weakens in proportion to the global warming amplitude, largely unaffected by SST pattern changes. Conversely, the Walker circulation response is sensitive to SST pattern changes, weakening with global warming if zonal SST contrast decreases or increases below a certain threshold and strengthening if the increase in SST contrast exceeds that threshold. Thus, the Walker circulation might continue to strengthen if the SST pattern effects dominate. Our results indicate that the weakening of convective mass flux alone is insufficient for projecting the Walker circulation response.

Plain Language Summary Global warming is known to weaken both the convective mass flux and the Walker circulation. Yet, in the past decades, the convective mass flux has been weakening while the Pacific Walker circulation has actually been strengthening. To investigate this discrepancy, we conducted a series of experiments with varying SSTs. Our results reveal that the convective mass flux weakens with global warming, largely unaffected by SST pattern changes. On the other hand, the Walker circulation's response is greatly influenced by SST patterns; it can strengthen if the zonal SST contrast across the tropical Pacific is sufficiently large, despite global warming. This suggests that accurately projecting the Walker circulation requires a better understanding of SST pattern changes.

1. Introduction

The Walker circulation is a large-scale atmospheric circulation in the tropical Pacific characterized by ascent in the western Pacific warm pool and descent in the central-to-eastern Pacific cold tongue. Under global warming, the Walker circulation is projected to weaken associated with a reduced zonal gradient of sea surface temperature (SST) along the equatorial Pacific (Duffy & O'Gorman, 2023; Vecchi et al., 2006). Several factors can lead to larger warming in the eastern than in the western tropical Pacific in response to CO_2 forcing. First, radiative forcing in the warm western Pacific can be more effectively balanced by evaporative fluxes compared to the cold eastern Pacific because evaporative fluxes increase exponentially with temperature (i.e., Clausius-Clapeyron relation). This evaporative damping mechanism leads to enhanced warming in the east (Knutson and Manabe, 1995). Second, the western tropical Pacific is subject to more efficient radiative damping as enhanced convection due to warming is accompanied by strong shortwave cloud radiative effect, unlike the eastern tropical Pacific, which lacks such damping mechanisms (Park et al., 2022). Third, the warm water subducted in the subtropics upwells in the eastern Pacific (Gu & Philander, 1997; Heede et al., 2020), and this ocean tunnel mechanism leads to more warming in the eastern than in the western tropical Pacific.

In contrast, other mechanisms also exist that increase the zonal SST gradient in the tropical Pacific in response to CO_2-induced warming. For example, warming in the tropical Atlantic or Indian Ocean causes cooling in the eastern tropical Pacific via enhanced trade winds (Li et al., 2016; J.-J. Luo et al., 2012). Also, equatorial upwelling in the eastern Pacific can dampen surface warming and therefore strengthen the zonal SST gradient (Clement et al., 1996). This mechanism called the ocean dynamical thermostat, however, is only effective in the fast timescales shorter than the advective timescale of ocean subtropical cells (i.e., less than 10 years after an abrupt CO_2 increase) (Y. Luo et al., 2017). Despite these compensating mechanisms, most models robustly project a weaker zonal SST gradient and weaker Walker circulation, particularly on long timescales. Although these

projections are argued to be erroneous due to common equatorial cold tongue bias (Seager et al., 2019), many lines of evidence suggest that a weakening of the Walker circulation is plausible on slow timescales (Watanabe et al., 2024).

In addition to the weakening of the Walker circulation, another robust feature of global warming is the weakening of convective mass flux. This weakening is explained by a global hydrological constraint as the rate of precipitation increase is smaller than the rate of specific humidity increase (Held & Soden, 2006). The weakening of convective mass flux has often been used to explain the weakening of the Walker circulation under global warming (e.g., Vecchi et al., 2006). However, Held and Soden (2006) explicitly state that *a reduction in the mass exchange in the tropics does not necessarily entail a proportional reduction in the strength of the mean tropical circulation*. Indeed, the Walker circulation and convective mass flux are not always tied together. During the past several decades after around 1979, despite modest global warming, the Walker circulation and convective mass flux have exhibited opposite trends: the Walker circulation has strengthened while the convective mass flux has weakened (Shrestha & Soden, 2023; Watanabe et al., 2023). This period is characterized by an enhanced zonal SST gradient with strong cooling over the eastern tropical Pacific. Hence, the SST pattern effect of strengthening the Walker circulation likely has over-compensated the global warming effect of weakening the Walker circulation (Watanabe et al., 2023). This raises the question of whether the Walker circulation response can be directly linked to convective mass flux changes. This notion has been challenged by Sandeep et al. (2014), who demonstrated that a Walker circulation trend of either sign could occur alongside a weakening convective mass flux. We aim to clarify the relationship between the Walker circulation and convective mass flux by disentangling the effects of SST patterns and global warming on both.

2. Data and Methods

2.1. Model and Experiment Design

We employ the general circulation atmosphere model, ECHAM6.3 (Stevens et al., 2013), which is a spectral model at T63 horizontal resolution (corresponding to 96 × 192 Gaussian longitude–latitude grids; approximately 210 km at the equator) with 47 vertical levels extending to 0.01 hPa. We prescribe constant radiative forcing parameters: atmospheric greenhouse gas concentrations represent the time period between 1979 and 2013 (CO_2: 363.689 ppmv, CH_4: 1703.97 ppbv, N_2O: 313.056 ppbv) and ozone and aerosol concentrations are prescribed to monthly climatologies for the year 1996. Orbital parameters are fixed to the year 1996. Additionally, land use change and vegetation dynamics are switched off.

In the control experiment, SST and sea ice concentration are prescribed as monthly climatologies derived from PCMDI AMIP forcing data averaged over the years 1979–2013. We then perform a series of time-slice prescribed SST experiments to differentiate the effect of global warming and SST pattern changes. We consider the SST pattern changes between 1979 and 2013 by taking the linear trend of monthly SST multiplied by 35 × 12 (months), with the global-mean trend of 0.24 K removed uniformly. The experiment, denoted pHIST+0K, is forced by this SST anomaly pattern added to the control SST profile (Figure S1a in Supporting Information S1). The other experiment, denoted nHIST+0K, is similar to pHIST+0K, except that the SST anomaly is reversed in sign (Figure S1b in Supporting Information S1). The global warming effect is considered by additionally adding a uniform SST warming of varying degrees of 2, 4, and 6 K. For example, the experiment with the SST anomaly of pHIST pattern and a uniform warming of 2 K is denoted as pHIST+2K. The zonal SST contrast is enhanced over the tropical Pacific in the pHIST experiments and decreased in the nHIST experiments. We also perform the experiments, denoted as UNI, in which the global SST is uniformly increased with no pattern changes. The sea ice cover is fixed to the control profile in all perturbed experiments.

All experiments are integrated for 24 years. The same monthly SST profile is repeated every year. The first 4 years are discarded before taking the time-mean for computing the climatology. The annual-mean climatology difference between the perturbed and control experiments is denoted as δ. The experiments with no global warming, pHIST+0K and nHIST+0K, highlights the SST pattern effect while the experiments with no SST pattern changes, UNI, highlights the global warming effect.

2.2. Diagnostics

We examine the direct output of sub-grid atmospheric net upward convective mass flux M_c. The resolved scale mass flux is represented by $M_{up} = 1/g \cdot A_{up}\omega_{up}$ where A_{up} is the fraction of the globe covered by ascent and ω_{up} is the global-mean ascending pressure velocity with the reversed sign so that M_{up} is positive definite (Jenney et al., 2020). We use daily mean data for computing M_{up}. The fractional change in M_{up} can be divided into the fractional change in A_{up} and ω_{up}, that is, $\Delta M_{up} = \Delta A_{up} + \Delta\omega_{up}$ where Δ denotes the fractional change relative to the control simulation, that is, the difference between the perturbed and control simulations (δ) divided by the control climatology. The fractional change in convective mass flux can be also estimated from global hydrological constraint as $\Delta M_c^* = \Delta P - \Delta q$ where P is global-mean precipitation and q is global-mean 2-m specific humidity (Held & Soden, 2006).

The Walker circulation strength is defined as the difference in sea level pressure (SLP) between the central/east Pacific (160°W−80°W, 5°S−5°N) and the Indian Ocean/west Pacific (80°E−160°E, 5°S−5°N), following Vecchi et al. (2006). This index is positive in the control climate, associated with low pressure over the ascending branch of the Walker circulation over the western Pacific warm pool and high pressure over the descending branch of the Walker in the central-eastern Pacific.

3. Convective Mass Flux Changes

Figure 1a compares the changes in global-mean convective mass flux at 600 hPa (ΔM_c) as a function of the response in global-mean surface air temperature. The size of circle symbols represents the amplitude of prescribed global-mean SST warming. The global-mean convective mass flux ΔM_c decreases proportional to the degree of global warming at a rate of -2.98 ± 0.14%/K when normalized by the global-mean surface air temperature changes. The results are qualitatively consistent regardless of the vertical level at which ΔM_c is diagnosed, but the magnitude of the percentage change per unit warming is sensitive to the vertical level, peaking in the mid-troposphere between 700 and 600 hPa (Fig. S2 in Supporting Information S1). The weakening of convective mass flux is consistent with the global-mean hydrological constraint but the latter estimate ΔM_c^* shows a larger sensitivity to global warming with -3.94 ± 0.43%/K (Figure 1b). The resolved scale mass flux ΔM_{up} also decreases with global warming, but at a significantly slower pace of -1.77 ± 0.24%/K at 600 hPa (Figure 1c). However, the relative amplitude of weakening rate between ΔM_c and ΔM_{up} depends on the vertical level (Figure S2 in Supporting Information S1). For example, at 500 hPa, ΔM_{up} weakens faster with global warming than ΔM_c. A decrease in ΔM_{up} is mainly due to a weakening of ascending velocity, with a relatively minor contribution from the narrowing of the ascending area (Figure S3 in Supporting Information S1).

Figures 1a–1c shows that global-mean atmospheric mass flux, irrespective of the definition (ΔM_c, ΔM_c^*, and ΔM_{up}), consistently weakens with global warming, although the magnitude of this weakening rate varies depending on the definition and the vertical level. The close agreement between the different colored lines indicates that they are largely independent of SST pattern changes. This tendency remains relevant even when the analysis is confined to the tropics where most atmospheric convection occurs: the global-mean ΔM_c is strongly correlated with the tropical ΔM_c averaged between 20°S and 20°N (Figure 1d). We now focus on the tropical ΔM_c given our aim to connect convective mass flux changes with large-scale Walker circulation changes.

Tropical-mean convective mass flux weakens with global warming regardless of SST pattern changes (Figure 1d). Does this also imply that the spatial pattern of convective mass flux changes δM_c is unaffected by SST pattern changes? Figure 2 compares the spatial map of δM_c between 20°S and 20°N. The pHIST+0K case exhibits M_c increase over the western Pacific where SST warming is prescribed and M_c decrease over the eastern Pacific where SST cooling is prescribed (Figure 2b), which nearly cancel out when averaged over the entire tropics (Figure 1d). The nHIST+0K case exhibits δM_c with the opposite sign compared to pHIST+0K due to the prescribed SST anomaly having a reversed sign (Figures 2b and 2c and Figure S1 in Supporting Information S1). Hence, the spatial correlation of δM_c between pHIST+0K and nHIST+0K is strongly negative at -0.61 (Figure 2a).

A uniform SST warming leads to a decrease in M_c almost everywhere in the tropics, with the largest reduction occurring over the Indo-Pacific warm pool, where the control climatology shows the maximum M_c (Figure 2d). As uniform SST warming is added to the pattern anomaly, the stark contrast in the decrease and increase of M_c

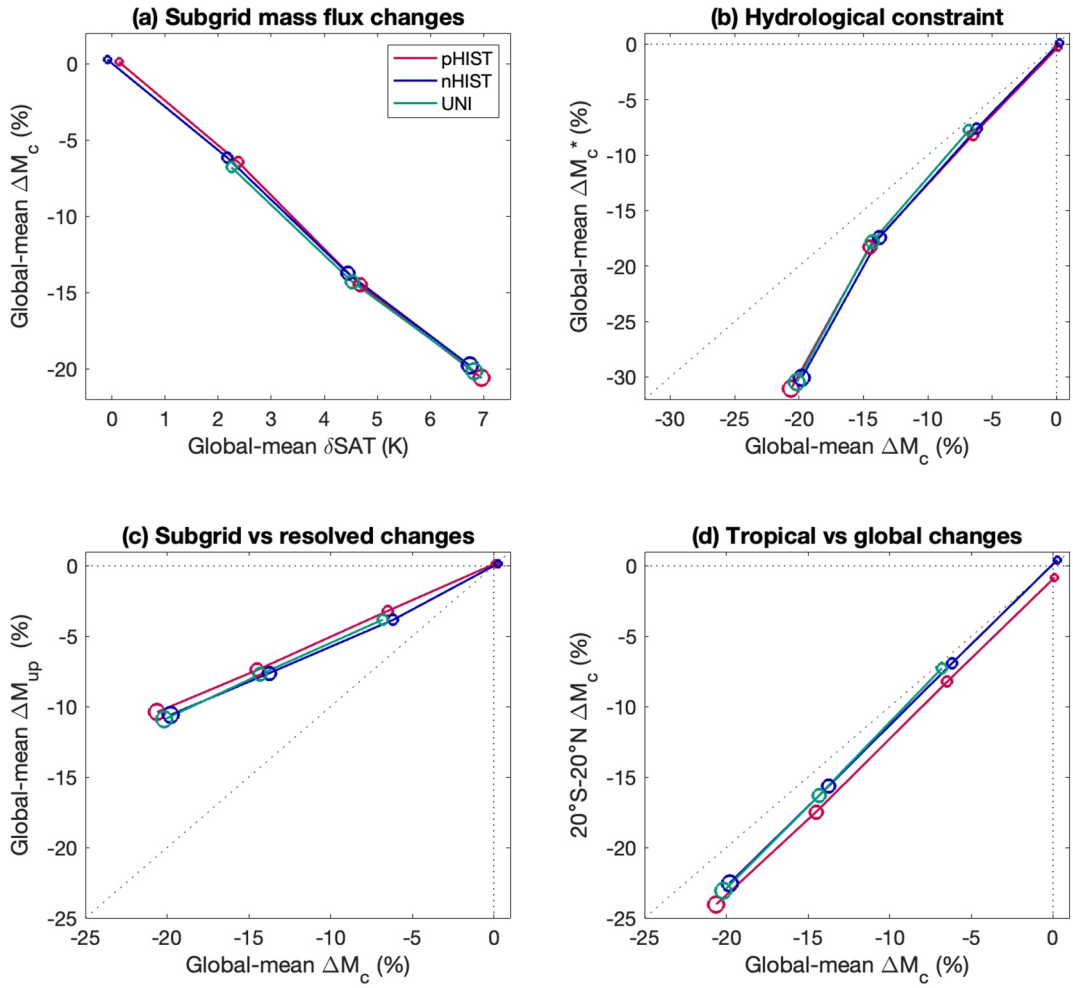

Figure 1. (a) Global-mean sub-grid scale convective mass flux change at 600 hPa, ΔM_c (in %) against global-mean surface air temperature change δ SAT (in K). (b) ΔM_c estimate from the global hydrological budget (i.e., $\Delta M_c^* = \Delta P - \Delta q$) against ΔM_c. (c) Resolved-scale ΔM_{up} against sub-grid scale ΔM_c. (d) Tropics-mean ΔM_c, averaged between 20°S and 20°N, against global-mean ΔM_c. The size of circle symbols corresponds to the prescribed global-mean SST warming amplitude (i.e., 0K, +2K, +4K, and +6K), with pHIST in red, nHIST in blue, and UNI in green.

within the tropics, evident in pHIST+0K and nHIST+0K, diminishes (Figures 2b–2f). Hence, the negative correlation weakens between pHIST and nHIST when a global SST warming of 2 K is added compared to 0 K (Figure 2a). The pattern effect gradually weakens with an increase in uniform SST warming as the tropics-wide decrease in M_c becomes more dominant. Consequently, the pattern correlation turns positive with sufficiently large uniform SST warming, reaching +0.44 for a 6 K warming (Figure 2a). That is, the spatial pattern of δM_c depends on both the SST anomaly pattern and the degree of global warming, with their relative importance varying with global warming amplitude. In contrast, the tropics-mean δM_c is primarily constrained by the global-mean warming amplitude and is relatively insensitive to the SST pattern (Figure 1d).

Nevertheless, a robust, albeit small, sensitivity exists in the tropics-mean δM_c to the SST pattern, such that pHIST exhibits a larger M_c weakening than nHIST for any given amplitude of global SST warming (Figure 1d). With global warming, the convective mass flux M_c weakens due to enhanced stability associated with moist adiabatic adjustment, leading to amplified warming in the upper tropical troposphere. Greater M_c weakening will be followed by larger warming in the upper troposphere, accompanying a larger rise in the tropopause height. Hence, the tropics-mean δM_c weakening is proportional to the increase in tropopause height, which is an indirect measure of increased stability (Figure 3a). For a given degree of global SST warming, the tropopause rises more in pHIST

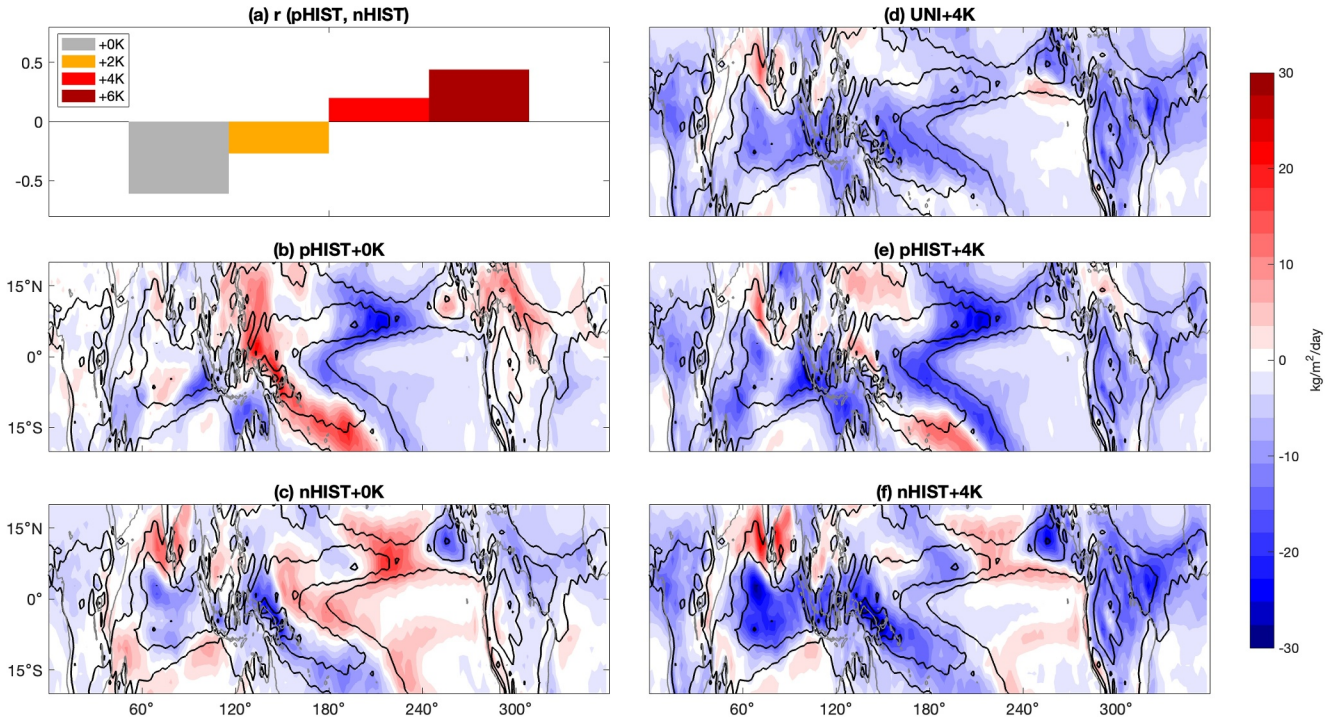

Figure 2. (a) Spatial correlation of tropics-mean δM_c between pHIST and nHIST with the prescribed global SST increase of 0K (gray), 2K (yellow), 4K (red), and 6K (dark red). Spatial map of δM_c (shading) and M_c climatology in the control experiment (contours, interval = 20 kg m^{-2} day^{-1}) in (b) pHIST+0K, (c) nHIST+0K, (d) UNI+4K, (e) pHIST+4K, and (f) nHIST+4K.

than nHIST, indicating a larger increase in static stability and consequently a larger reduction in M_c (Fan & Dommenget, 2024; Wills et al., 2017). The larger stability increase in pHIST occurs because the SST increase is prescribed over the climatological convection region, where the warming effect is communicated aloft and remotely warms the tropical free troposphere (Figure S4a in Supporting Information S1). In contrast, nHIST exhibits less stability increase because the SST increase is prescribed over the cold eastern Pacific, where the warming is trapped locally near the surface (Figure S4b in Supporting Information S1).

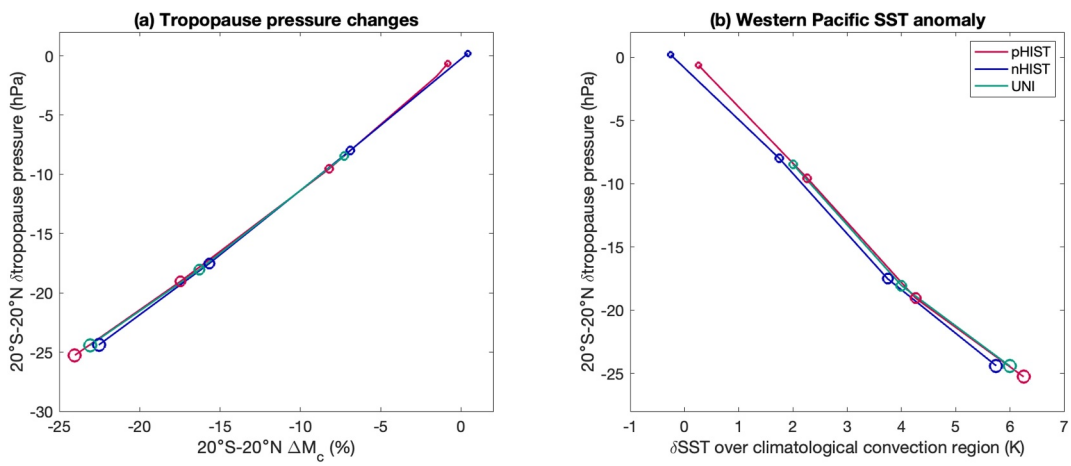

Figure 3. Tropopause pressure response averaged between 20°S−20°N (in hPa) against (a) tropics-mean ΔM_c (in %) and (b) prescribed SST anomaly (in K) averaged over the western Pacific with climatological ascending motions. The tropopause height, defined using a threshold lapse rate of 2 K km^{-1} (Reichler et al., 2003), is calculated using the Tropical-Width Diagnostics (TropD) code package in Adam et al. (2018). Figure format same as in Figure 1.

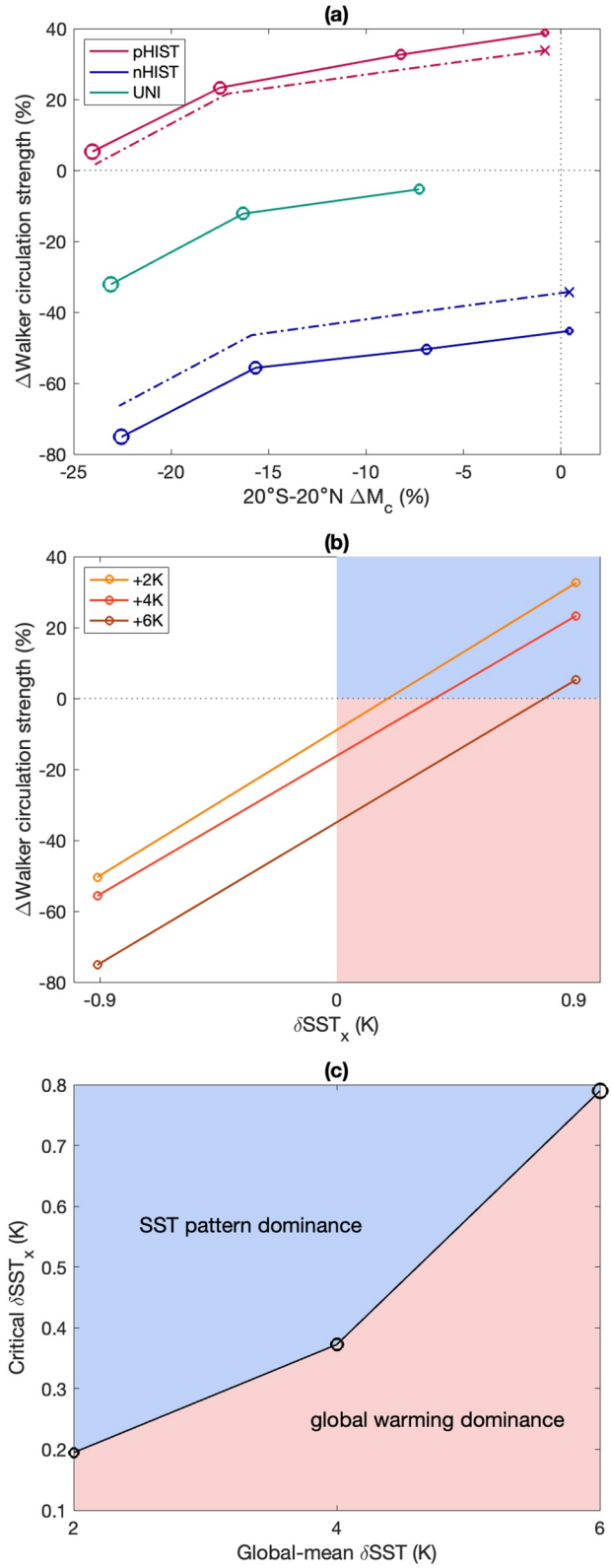

Figure 4.

4. Walker Circulation and Convective Mass Flux Changes

Figure 4a compares the tropical-mean convective mass flux changes with the Walker circulation strength changes. The Walker circulation strengthens by 38.8% in pHIST+0K, associated with enhanced zonal SST gradients along the equatorial Pacific, while it weakens by 45.3% in nHIST+0K. However, the tropical-mean convective mass flux change is minimal in both cases due to the absence of global-mean SST warming. For a given SST anomaly pattern, the Walker circulation weakens with global warming, as does the convective mass flux. It is also worth noting that uniform SST warming in UNI also leads to a weakening of the Walker circulation (Figure 4a), due to enhanced atmospheric stability (He & Soden, 2015). Moreover, the rate of Walker circulation weakening increases in a warmer climate: the same +2K leads to about 3 times larger weakening for UNI+4K compared to UNI+2K. However, changes in Walker circulation strength are not always consistent with changes in convective mass flux. The nHIST experiments show that both the Walker circulation and convective mass flux weaken, whereas the pHIST experiments show a Walker circulation strengthening alongside a convective mass flux weakening. Notably, the Walker circulation remains strengthening in pHIST+6K despite a global SST warming of 6 K. This underscores the significance of the pattern effect during the historical period of 1979–2013.

The changes in Walker circulation strength in pHIST+0K and nHIST+0K can be predicted using the Green's function experiment, where a patch of SST anomalies is prescribed to 91 locations globally (Alessi & Rugenstein, 2023). Despite some underestimation, the Green's function experiment using ECHAM6.3 (the same atmosphere model employed in this study) well reproduces the Walker circulation strengthening in pHIST+0K and weakening in nHIST+0K (crosses in Figure 4a). These predicted responses are added to the UNI response to replicate the pHIST and nHIST responses with non-zero global warming. The close agreement between the solid and dash-dot lines suggests that the Walker circulation response can be understood as the sum of the SST pattern effect, as predicted by the Green's function experiment, and the global warming effect, as simulated by the UNI experiments.

To distinguish the relative contributions of the SST pattern and global warming effects to Walker circulation changes, Figure 4b compares the changes in Walker circulation strength with the zonal contrast in the prescribed SST anomaly across the equator, between the longitudes 90°–140° and 180°–240°, $\delta\,\mathrm{SST_x}$. Positive $\delta\,\mathrm{SST_x}$ corresponds to pHIST experiments and negative $\delta\mathrm{SST_x}$ corresponds to nHIST experiments. The regime shaded in blue indicates where the Walker circulation strengthens despite global warming effect, as the SST pattern effect overwhelms. Conversely, the red-shaded regime shows where the Walker circulation weakens despite an enhanced zonal SST gradient, as the global warming effect dominates. Hence, changes in Walker circulation strength are not always aligned with changes in convective mass flux, particularly when the SST pattern effect dominates over the global warming effect. The *x*-intercept in Figure 4b represents the critical $\delta\mathrm{SST_x}$ at which the regime shifts from the global warming dominance to SST pattern dominance, as shown in Figure 4c. For a given degree of global warming, the Walker circulation weakens if the increase in zonal SST contrast is below the critical $\delta\mathrm{SST_x}$ and strengthens if it is above this threshold. The critical $\delta\mathrm{SST_x}$ increases with global warming as a larger increase in SST gradient is needed to compensate for the warming effect. The Walker circulation strengthening due to the enhanced $\delta\mathrm{SST_x}$ in pHIST, which corresponds to changes between 1979 and 2013, is so large that it cannot be compensated even by a global SST warming of 6 K (Figure 4b). The increase in $\delta\mathrm{SST_x}$ far exceeded the critical value for a global SST warming of 0.24 K during this period. In other words, the global warming effect was insufficient to offset the SST pattern effect, resulting in a strengthening of the Walker circulation.

5. Discussion

In this paper, we investigate the relationship between changes in the Walker circulation and convective mass flux in response to global warming and zonal SST gradient changes across the tropical Pacific, both separately and in

Figure 4. (a) Tropics-mean ΔM_c (in %) against Walker circulation strength changes (in %). Figure format same as in Figure 1. Walker circulation strength changes in pHIST+0K and nHIST+0K predicted from the Green's function experiment (crosses), and this prediction added to the response in UNI (dash-dot lines). (b) Walker circulation strength changes against the prescribed zonal SST gradient anomaly along the equatorial Pacific, $\delta\,\mathrm{SST_x}$. (c) The *x*-intercept of the lines in (b), indicating the critical zonal SST contrast required to cause a regime shift. In (b) and (c), red shading indicates the global warming dominating regime where the Walker circulation weakens despite enhanced zonal SST contrast and blue shading indicates the SST pattern dominating regime where the Walker circulation strengthens despite global warming.

combination, using a series of fixed SST experiments. Both the convective mass flux and Walker circulation weaken in proportion to the degree of global SST warming. While the SST pattern changes have little impact on the tropical-mean convective mass flux change, the Walker circulation is highly dependent on the SST pattern changes.

It is worth noting that the spatial pattern of convective mass flux changes does depend on the SST pattern changes, but the tropical average is constrained by the global warming amplitude. Hence, the tropical-mean convective mass flux change is negligible in the absence of global SST warming despite a prominent change in the tropical SST pattern. A small sensitivity of tropical-mean convective mass flux change to SST pattern exists because the western Pacific SST warming induces a larger increase in static stability throughout the tropical troposphere whereas the eastern Pacific SST warming has limited impact on the static stability due to the locally confined warming effect. Hence, for the same degree of global SST warming, the western Pacific amplified SST warming pattern accompanies a slightly greater weakening of tropical-mean convective mass flux relative to the eastern Pacific amplified SST warming pattern.

In contrast, the Walker circulation responds sensitively to tropical Pacific SST pattern changes. In the presence of reduced zonal SST gradient, both the SST pattern and global warming effects act together to weaken the Walker circulation. Conversely, in the presence of enhanced zonal gradient, the SST pattern effect acts to strengthen the Walker circulation while the global warming effect acts to weaken the Walker circulation. As the two effects are opposing each other, there are two regimes where one of the other dominates. Consider the case in which the SST gradient increases with global warming. If the SST gradient increase is larger than a threshold, the global warming effect is overcompensated to result in Walker circulation strengthening. If SST gradient increase is smaller than a threshold, the SST pattern effect is overcompensated to result in Walker circulation weakening. The threshold SST gradient that divides the two regimes increases with the amplitude of global warming.

Our results suggest that, in the past decades, the increase in the zonal SST gradient exceeded the threshold for the observed global SST warming of 0.24 K. This led to the Walker circulation strengthening despite the concurrent weakening of the convective mass flux. In global warming scenario, the majority of models project the zonal SST gradient to decrease in the slow timescale (Heede et al., 2020), indicating that both the SST pattern and global warming effects will work together to weaken the Walker circulation and convective mass flux. However, it remains uncertain how the tropical Pacific SST pattern will change, necessitating that projections of Walker circulation take into account potential SST pattern changes. With larger global warming, the SST gradient threshold increases, making it more likely that the Walker circulation will weaken in the long term. In near-term projections, however, the SST gradient threshold is smaller and several mechanisms exist that could enhance the zonal SST gradient, potentially allowing the Walker circulation to continue strengthening. Thus, both the SST pattern and global warming effects need to be considered when explaining changes in the Walker circulation, and only the component related to global warming effect is linked to the convective mass flux. Hence, the weakening of convective mass flux alone is insufficient to explain the weakening of the Walker circulation.

The convective mass flux weakening has consistently been linked to a robust weakening of the global-mean atmospheric circulation in the zonally asymmetric component rather than the zonal-mean (Held & Soden, 2006; Shrestha & Soden, 2023; Vecchi & Soden, 2007). This relationship holds in our experiments, regardless of SST patterns (Fig. S5 in Supporting Information S1). Our findings indicate that the weakening of zonally asymmetric circulation does not necessarily manifest as a weakening of the Walker circulation. Further investigation is needed to identify which other modes of zonally asymmetric circulations are responsible for this weakening.

Conflict of Interest

The authors declare no conflicts of interest relevant to this study.

Data Availability Statement

The Max Planck Earth system model MPI-ESM1.2 is subject to the Custom Data set Terms detailed at Model Development Team Max-Planck-Institut für Meteorologie (2024). The source code version we used in this study as well as the scripts for preprocessing, model execution, postprocessing and analysis of the results are available

from Edmond, the Open Research Data Repository for the Max Planck Society (Gayler, 2024). Data for this study is subject to the terms of the Creative Commons Attribution 4.0 International (CC BY 4.0) license and can be found at Kang and Gayler (2024), in the German Climate Computing Center (DKRZ) long-term archive for documentation.

Acknowledgments
M.W. was supported by the Program for Advanced Studies of Climate Change Projection (SENTAN) Grant-in-Aid JPMXD0722680395 from the Ministry of Education, Culture, Sports, Science and Technology (MEXT) and JSPS Kakenhi Grant 24H00261, Japan. Open Access funding enabled and organized by Projekt DEAL.

References

Adam, O., Grise, K. M., Staten, P., Simpson, I. R., Davis, S. M., Davis, N. A., et al. (2018). The TropD software package (v1): Standardized methods for calculating tropical-width diagnostics. *Geoscientific Model Development*, *19*.

Alessi, M. J., & Rugenstein, M. A. A. (2023). Surface temperature pattern scenarios suggest higher warming rates than current projections. *Geophysical Research Letters*, *50*(23), e2023GL105795. https://doi.org/10.1029/2023GL105795

Clement, A. C., Seager, R., Cane, M. A., & Zebiak, S. E. (1996). An Ocean dynamical thermostat. *Journal of Climate*, *9*, 2190–2196. https://doi.org/10.1175/1520-0442(1996)009<2190:aodt>2.0.co;2

Duffy, M. L., & O'Gorman, P. A. (2023). Intermodel spread in Walker circulation responses linked to spread in moist stability and radiation responses. *Journal of Geophysical Research: Atmospheres*, *128*(1), e2022JD037382. https://doi.org/10.1029/2022JD037382

Fan, C.-S., & Dommenget, D. (2024). The weakening of the tropical circulation is caused by the lifting of the tropopause height. *Climate Dynamics*, *62*(1), 187–201. https://doi.org/10.1007/s00382-023-06909-1

Gayler, V. (2024). MPIESM-1.2 model version and scripts used to examine convective mass flux and Walker circulation changes [Software]. *Edmond*. https://doi.org/10.17617/3.GVZJRT

Gu, D., & Philander, S. G. H. (1997). Interdecadal climate fluctuations that depend on exchanges between the tropics and extratropics. *Science*, *275*(5301), 805–807. https://doi.org/10.1126/science.275.5301.805

He, J., & Soden, B. J. (2015). Anthropogenic weakening of the tropical circulation: The relative roles of direct CO2 forcing and sea surface temperature change. *Journal of Climate*, *28*(22), 8728–8742. https://doi.org/10.1175/JCLI-D-15-0205.1

Heede, U. K., Fedorov, A. V., & Burls, N. J. (2020). Time scales and mechanisms for the tropical Pacific response to global warming: A Tug of war between the ocean thermostat and weaker Walker. *Journal of Climate*, *33*(14), 6101–6118. https://doi.org/10.1175/JCLI-D-19-0690.1

Held, I. M., & Soden, B. J. (2006). Robust responses of the hydrological cycle to global warming. *Journal of Climate*, *19*(21), 5686–5699. https://doi.org/10.1175/JCLI3990.1

Jenney, A. M., Randall, D. A., & Branson, M. D. (2020). Understanding the response of tropical ascent to warming using an energy balance framework. *Journal of Advances in Modeling Earth Systems*, *12*(6), e2020MS002056. https://doi.org/10.1029/2020MS002056

Kang, S. M., & Gayler, V. (2024). MPIESM-1.2 model output used to examine convective mass flux and Walker circulation changes [Dataset]. *DOKU at DKRZ*. https://www.wdc-climate.de/ui/entry?acronym=DKRZ_LTA_1421_ds00001

Knutson, T. R., & Syukuro, M. (1995). Time-mean response over the tropical Pacific to increased CO2 in a coupled ocean-atmosphere model. *Journal of Climate*, *8*(9), 2181–2199. https://doi.org/10.1175/1520-0442(1995)008<2181:TMROTT>2.0.CO;2

Li, X., Xie, S.-P., Gille, S. T., & Yoo, C. (2016). Atlantic-induced pan-tropical climate change over the past three decades. *Nature Climate Change*, *6*(3), 275–279. https://doi.org/10.1038/nclimate2840

Luo, J.-J., Sasaki, W., & Masumoto, Y. (2012). Indian Ocean warming modulates Pacific climate change. *Proceedings of the National Academy of Sciences*, *109*(46), 18701–18706. https://doi.org/10.1073/pnas.1210239109

Luo, Y., Lu, J., Liu, F., & Garuba, O. (2017). The role of ocean dynamical thermostat in delaying the El Niño–Like response over the equatorial Pacific to climate warming. *Journal of Climate*, *30*(8), 2811–2827. https://doi.org/10.1175/JCLI-D-16-0454.1

Model Development Team Max-Planck-Institut für Meterologie. (2024). MPI-ESM 1.2.01p7 [Software]. *Edmond*. https://doi.org/10.17617/3.H44EN5

Park, C., Kang, S. M., Stuecker, M. F., & Jin, F.-F. (2022). Distinct surface warming response over the western and eastern equatorial Pacific to radiative forcing. *Geophysical Research Letters*, *49*(2). https://doi.org/10.1029/2021GL095829

Reichler, T., Dameris, M., & Sausen, R. (2003). Determining the tropopause height from gridded data. *Geophysical Research Letters*, *30*(20), 2003GL018240. https://doi.org/10.1029/2003GL018240

Sandeep, S., Stordal, F., Sardeshmukh, P. D., & Compo, G. P. (2014). Pacific Walker Circulation variability in coupled and uncoupled climate models. *Climate Dynamics*, *43*(1–2), 103–117. https://doi.org/10.1007/s00382-014-2135-3

Seager, R., Cane, M., Henderson, N., Lee, D.-E., Abernathey, R., & Zhang, H. (2019). Strengthening tropical Pacific zonal sea surface temperature gradient consistent with rising greenhouse gases. *Nature Climate Change*, *9*(7), 517–522. https://doi.org/10.1038/s41558-019-0505-x

Shrestha, S., & Soden, B. J. (2023). Anthropogenic weakening of the atmospheric circulation during the satellite era. *Geophysical Research Letters*, *50*(22), e2023GL104784. https://doi.org/10.1029/2023GL104784

Stevens, B., Giorgetta, M., Esch, M., Mauritsen, T., Crueger, T., Rast, S., et al. (2013). Atmospheric component of the MPI-M Earth system model: ECHAM6. *Journal of Advances in Modeling Earth Systems*, *5*(2), 146–172. https://doi.org/10.1002/jame.20015

Vecchi, G. A., & Soden, B. J. (2007). Global warming and the weakening of the tropical circulation. *Journal of Climate*, *20*(17), 4316–4340. https://doi.org/10.1175/JCLI4258.1

Vecchi, G. A., Soden, B. J., Wittenberg, A. T., Held, I. M., Leetmaa, A., & Harrison, M. J. (2006). Weakening of tropical Pacific atmospheric circulation due to anthropogenic forcing. *Nature*, *441*(7089), 73–76. https://doi.org/10.1038/nature04744

Watanabe, M., Iwakiri, T., Dong, Y., & Kang, S. M. (2023). Two competing drivers of the recent Walker circulation trend. *Geophysical Research Letters*, *50*(23), e2023GL105332. https://doi.org/10.1029/2023GL105332

Watanabe, M., Kang, S. M., Collins, M., Hwang, Y.-T., McGregor, S., & Stuecker, M. F. (2024). Possible shift in controls of the tropical Pacific surface warming pattern. *Nature*, *630*(8016), 315–324. https://doi.org/10.1038/s41586-024-07452-7

Wills, R. C., Levine, X. J., & Schneider, T. (2017). Local energetic constraints on Walker circulation strength. *Journal of the Atmospheric Sciences*, *74*(6), 1907–1922. https://doi.org/10.1175/JAS-D-16-0219.1